

Supplemental Information: An acoustic black hole in a stationary hydrodynamic flow of microcavity polaritons

H. S. Nguyen^{1,*}, D. Gerace², I. Carusotto³, D. Sanvitto⁴,
E. Galopin¹, A. Lemaître¹, I. Sagnes¹, J. Bloch¹, and A. Amo¹

¹*Laboratoire de Photonique et de Nanostructures,
LPN/CNRS, Route de Nozay, 91460 Marcoussis, France*

²*Dipartimento di Fisica, Università di Pavia, via Bassi 6, I-27100 Pavia, Italy*

³*INO-CNR BEC Center and Dipartimento di Fisica, Università di Trento, I-38123 Povo, Italy and*

⁴*NNL, Istituto Nanoscienze - CNR, Via Arnesano, 73100 Lecce, Italy*

(Dated: November 17, 2014)

I. EXPERIMENTAL SETUP AND SAMPLE CHARACTERIZATION

We adopt a transmission geometry (excitation and emission are collected from opposite sides of the sample) in order to avoid the stray light of the excitation laser. A scheme of the experimental setup is depicted in Fig. S1(a). This configuration allows us to image at the same time the photoluminescence of the polariton fluid in real-space and momentum-space, with or without spectral selection. Complemented with a suitable photon correlator to extract the photon statistics within the images, this configuration appears suitable to experimentally detect the non-trivial intensity correlation signal due to the analog Hawking radiation.

The polariton dispersion in the upstream and downstream regions is measured via non-resonant photoluminescence of the flat parts of the microstructure [Fig. S1.(b)]. The excitation energy is 72 meV blue-detuned with respect to the exciton energy, $E_{\text{ex}} = 1477.7$ meV. Figure S1(b) shows the photoluminescence from both the polariton modes and the uncoupled excitons emitting through the wire-edge. From the photoluminescence spectrum, we extract a detuning $\delta = E_{\text{cav}} - E_{\text{ex}} \approx -3$ meV, and a polariton effective mass $m \sim 3 \times 10^{-5} m_{\text{el}}$ (for a parabolic approximation of the lower polariton branch around $k = 0$), where m_{el} represents the free electron mass.

To characterize the shape of the excitation spot, we measure the spatial profile of the total emission along the wire axis, at very low excitation power, as depicted in Fig. S1(c). Thus the excitation spot is a gaussian with a full width at half maximum of $\sim 16.5 \mu\text{m}$.

In order to measure the selected emission in momentum space from the upstream or downstream regions, we spatially filter the emission from the desired region with the use of a slit located onto an intermediate image of the wire [Fig. S1.(a)]. The use of the slit induces a diffraction effect in the far-field images, particularly when we use a filter of $20 \mu\text{m}$ in width, which is the case in the upstream

measurements. This explains the broadening of the peaks in Figs. 2(a-c) of the main text compared to those in Figs. 2(d-f), for which the filter was $> 45 \mu\text{m}$ wide. Diffraction features are clearly evidenced in Fig. S1(d) which represents the data of Fig. 2(c) in logarithmic scale. We observe not only a central peak but also side peaks that are perfectly fitted by a Fraunhofer diffraction formula: $I = \sin^2 [w(k_{\text{fluid}} - k_y)/2] / [w(k_{\text{fluid}} - k_y)/2]^2$ with $w = 20.3 \mu\text{m}$ and $k_{\text{fluid}} = 0.2 \mu\text{m}^{-1}$. This shows that the side peaks in Fig. 2(c) do not originate from the backscattering of polaritons but are due to the diffraction of the central peak by the spatial selection slit.

II. INTERACTION ENERGY IN THE SUPERFLUID REGIME

The superfluid regime is achieved if the polariton fluid is subsonic ($v < c$). This condition is equivalent to:

$$E_{\text{int}} > 2E_{\text{kinetic}}, \quad (\text{S1})$$

where $E_{\text{int}} = mc^2$ is the interaction energy and $E_{\text{kinetic}} = mv^2/2$ is the kinetic energy of the polariton fluid in the single-particle picture. Moreover, as discussed in the main text, the total polariton energy is fixed by the excitation laser frequency [1], which implies that

$$E_{\text{pump}} = E_0 + E_{\text{kinetic}} + E_{\text{int}}, \quad (\text{S2})$$

where E_0 is the single-particle polariton energy at $k_y = 0$ [see Fig. 1(b) of the main text]. Therefore, in the superfluid regime the interaction energy satisfies:

$$E_{\text{int}} > \frac{2}{3} (E_{\text{pump}} - E_0) \quad (\text{S3})$$

III. PUMP-PROBE MEASUREMENTS IN THE DOWNSTREAM REGION

Polariton interactions in the black hole regime result in significant renormalizations of the polariton branches, following the Bogoliubov dispersion [1]. In order to evidence this effect and confirm our interpretation in terms of speeds of sound of the polariton fluid, we measure

* hai.son.nguyen@lpn.cnrs.fr; Present address: Institut de Nanotechnologies de Lyon, Ecole Centrale de Lyon, CNRS (UMR 5270), 36 avenue Guy de Collongue, 69134 Ecully, France

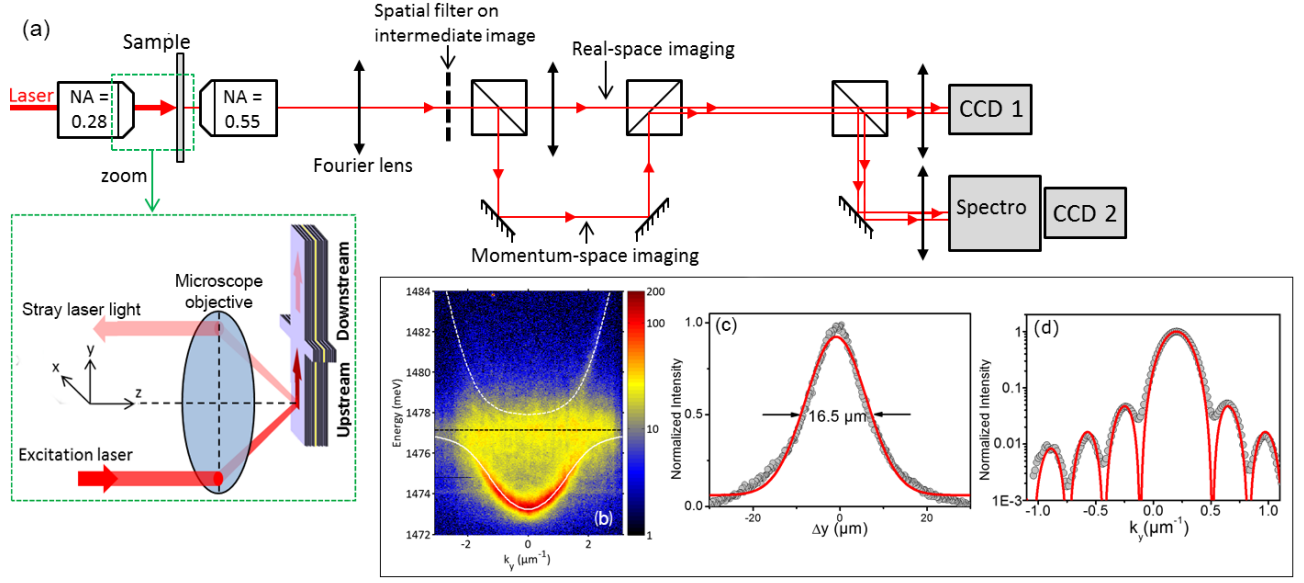


FIG. S1. (a) Scheme of the experimental setup. (b) Photoluminescence of the polariton wire under non-resonant excitation, showing the linear polariton dispersion. Dotted-black line: bare exciton energy. Dotted-white line (solid-white line): fit of the lower (upper) polariton branch from a two-coupled oscillators model. (c) Measured spatial profile of the integrated photoluminescence emission under non-resonant excitation. Red line: gaussian fit with FWHM = 16.5 μm . (d) Measured momentum distribution of the superfluid in the upstream region at pump power $p = 100$ mW [see also Fig. 2(c) of the main text], presented in semilogarithmic-scale. Red line: fit to a Fraunhofer diffraction response through a 20 μm -wide slit. The fitting parameters are $w = 20.3$ μm and $k_{\text{fluid}} = 0.2$ μm^{-1} .

the spectrum of excitations of the downstream fluid in a pump-probe experiment. The pump power is fixed at $p = 100$ mW in the upstream region in the conditions for the realization of the acoustic horizon. A second cw Ti:Sapphire laser at a slightly different energy and weak power $p_{\text{probe}} = 5$ mW, playing the role of a probe, is focused onto a 30 μm spot in the downstream region [see Fig. S2(a)]. Polariton emission at the energy of the probe laser is collected in transmission geometry.

As suggested in a slightly different context [2], the probe laser is used here to excite a propagating wave on top of the polariton fluid, similar to pouring a cup of water on top of a flowing river. Thus, the spectrum of excitations of the fluid can be reconstructed by measuring the wave vector k of the propagating wave excited by the probe and the wave vector k' of the part of the wave reflected against the defect, at different energies of the probe laser, E_{probe} . The emission of the background

fluid is filtered out with the use of a spectrometer. Figure S2(b) depicts the probe signal as a function of the wave vector, with $E_{\text{probe}} = E_{\text{pump}} - 0.21$ meV. We observe that the excited wave propagates at smaller wave vectors in the presence of the pump. Indeed, this effect is due to the renormalization of the spectrum of excitations due to the presence of the pump fluid in the nonlinear regime. The observation of excited modes below the pump energy is a clear evidence of the supersonic regime [4]. By repeating the same measurements at different E_{probe} values, we are able to reconstruct the dispersion in the downstream region, both in the linear (i.e. without pump) and nonlinear (i.e. in the presence of the pump) regimes [see Fig. S2(c)]. The dispersion in the linear regime corresponds well to the parabola $E(k_y) = E_0 + \hbar^2 k_y^2 / 2m$, while the dispersion in the nonlinear regime follows the expected positive branch of the Bogoliubov dispersion [1, 5]:

$$E_{\pm}(k_y) = E_{\text{pump}} \pm \frac{\hbar^2}{2m} \sqrt{(k_y - k_{\text{fluid}})^2 \left[(k_y - k_{\text{fluid}})^2 + \frac{2m}{\hbar} gn \right]} + \frac{\hbar^2 k_{\text{fluid}} (k_y - k_{\text{fluid}})}{m}, \quad (\text{S4})$$

where $k_{\text{fluid}} = 0.52$ μm^{-1} and $E_{\text{int}} = \hbar gn = 50$ μeV are the wavevector and interaction energy of the downstream fluid, respectively, corresponding to a pump power $p =$

100 mW [see Figs. 2(f) and 3(a) of the main text]. The same experiment, but measured in the upstream region, is technically more difficult since the probe signal is

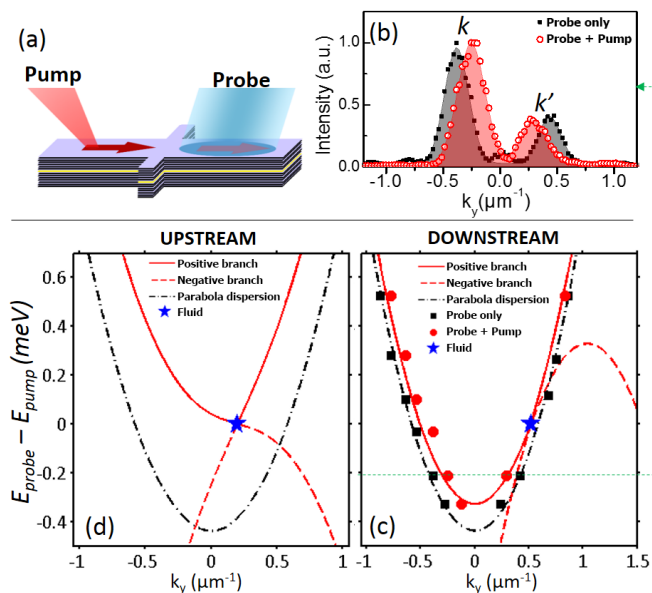


FIG. S2. (a) Sketch of the pump-probe experiment to measure the dispersion of excitations in the downstream region of the polariton fluid. (b) Momentum distribution of the photoluminescence at the probe frequency with (empty red circles) and without (black squares) the pump. The probe energy is fixed as $E_{\text{probe}} = E_{\text{pump}} - 0.21$ meV. A spatial filter from $y = 5 \mu\text{m}$ to $y = 30 \mu\text{m}$ is used to isolate the light emission from the downstream region, where $y = 0$ corresponds to the position of the defect. (c) Measured excitation spectrum in the downstream region obtained from the position of the k -space peak (b) with (red circles) and without (black squares) pump. The solid red line shows the Bogoliubov spectrum of excitations in the downstream region, calculated by using the positive branch of Eq. S4 with the measured k_{fluid} and E_{int} ; the dashed red line shows the corresponding negative branch. The black dash-dotted line shows the single-particle spectrum within the parabolic approximation, to which the Bogoliubov dispersion reduces in the absence of the pump. (d) Bogoliubov dispersion in the upstream region, calculated by inserting the values of k_{fluid} and E_{int} measured at $p = 100$ mW into Eq. S4.

washed out by the dominant fluid emission even with the use of a spectrometer. Nevertheless, we can calculate the excitation spectrum of the upstream fluid using the Bogoliubov dispersion S4 with the parameters measured at $p = 100$ mW ($k_{\text{fluid}} = 0.21 \mu\text{m}^{-1}$ and $\hbar g n = 0.35$ meV) as shown in Fig. S2(d). This dispersion, calculated with the measured parameters presented in the main text, corresponds to that of a subsonic fluid, indeed.

IV. ESTIMATION OF THE HAWKING TEMPERATURE

From the interaction energy above 100 mW [Fig. 3(a) of the main text], we estimate an average healing length

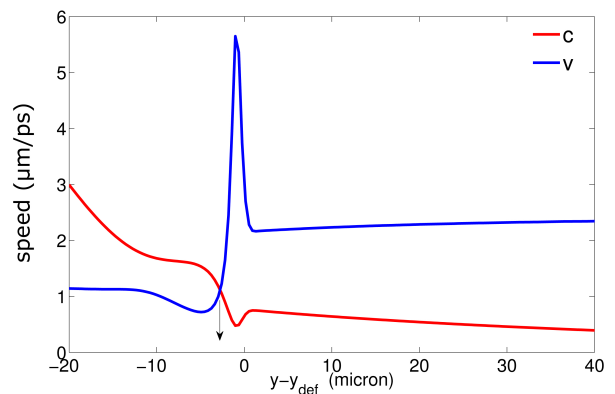


FIG. S3. Velocity profile as a function of propagation direction. The origin corresponds to the center position of the microstructured defect. The subsonic/supersonic boundary actually occurs about $2 \mu\text{m}$ on its negative side (see arrow).

of:

$$\xi \approx \frac{\hbar}{2\sqrt{m}} \left(\frac{1}{\sqrt{E_{\text{int}}^u}} + \frac{1}{\sqrt{E_{\text{int}}^d}} \right) \approx 1.5 \mu\text{m}. \quad (\text{S5})$$

where $E_{\text{int}}^{u(d)}$ is the interaction energy in the upstream (downstream) region. Since the horizon ($d \approx 8 \mu\text{m}$, see Fig. 1(g) in the main text) is smoother than the healing length ($d \gg \xi$), a Hawking temperature can be estimated in the hydrodynamic approximation [6]:

$$T_H \approx \frac{\hbar}{k_B d} \frac{(v_d^2 - c_d^2) - (v_u^2 - c_u^2)}{c_u + c_d} \approx 3 \text{ K} \quad (\text{S6})$$

where $v_{u(d)}$ and $c_{u(d)}$ are the measured fluid velocity and speed of sound in the upstream (downstream) region for an excitation power of 100 mW [see Fig. 3(b,c) in the main text]. In the case of polaritons, the characteristic energy with which this temperature should be compared is not the lattice or polariton temperature. Actually, polaritons are very weakly coupled to phonons in the semiconductor matrix and, when excited resonantly, their energy distribution is at most determined by their lifetime [7]. Therefore, T_H should be compared to the polariton lifetime. In the present sample, the polariton lifetime corresponds to a linewidth of $\sim 50 \mu\text{eV}$, i.e. much smaller than the thermal energy associated to the expected Hawking radiation ($\sim 250 \mu\text{eV}$ for 3 K). A difficulty in the observation of Hawking radiation could come from the shot noise in the photo-detection process, but this issue can be overcome with a sufficiently long integration time.

V. NUMERICAL SIMULATIONS I: DENSITY AND VELOCITY PROFILES

We have modeled this experiment by a driven-dissipative Gross-Pitaevskii equation, or generalized non-

linear Schrodinger equation. In particular, considering that we work very close to the bottom of the lower polariton dispersion, we restrict our model to a single field describing the lower polariton. Of course, it is implicit that the polariton is a composite quasi-particle, and the radiation detected is only related to its photonic component [1].

$$i \frac{d}{dt} \phi(y, t) = \left[\omega(-i\partial_y) + V(y) + g|\phi(y, t)|^2 - i\frac{\gamma}{2} \right] \phi(y, t) + F_{\text{pump}}(y, t), \quad (\text{S7})$$

which generalizes to the non-equilibrium context of polaritons the well-known Gross-Pitaevskii equation (GPE) of dilute Bose condensed gases [8]. In Eq. S7, $V(y)$ is the spatially-dependent potential for polaritons propagating along the microwire axis, y , obtained from the lateral shape of the studied wire (i.e., describing the microstructured defect), $\omega(-i\partial_y)$ describes the polariton dispersion (approximated with a free-particle dispersion with constant effective mass as measured close to the bottom polariton branch, see main text), g is the one-dimensional polariton-polariton interaction constant (assumed $0.3 \mu\text{eV}\cdot\mu\text{m}$ in these simulations, as appropriate for a microwire width of $3 \mu\text{m}$), and $F_{\text{pump}}(y, t) = F_0(y) \exp[i(k_{\text{pump}}y - \omega_{\text{pump}}t)]$ describes the gaussian pump spot in continuous wave excitation regime. The only fitting parameter in the simulations is the absolute value of the pump intensity.

The numerical solution of Eq. S7 allows to determine the fluid velocity and speed of sound along the wire axis, defined as $v(y) = \hbar \text{Im}(\phi^* \partial_y \phi) / m$ and $c(y) = \sqrt{\hbar g n(y) / m}$, respectively. In particular, for the microstructure under investigation and at high pump power (corresponding to the $p = 100 \text{ mW}$ experimental value, see the main text) the results are shown in Fig. 3, clearly

$$i d\phi = \left[\omega(-i\partial_y) + V(y) + g \left(|\phi|^2 - \frac{1}{\Delta y} \right) - i\frac{\gamma}{2} \right] \phi dt + F_{\text{pump}}(y, t) dt + \frac{\sqrt{\gamma}}{\sqrt{4\Delta y}} d\xi, \quad (\text{S8})$$

where Δy is the spacing of the real-space grid, and $d\xi$ is a complex valued, zero-mean, independent Gaussian noise term with white noise correlation in both space and time, i.e. $\overline{d\xi^*(y, t) d\xi(y', t)} = 2\delta(y - y') dt$. The equal-time spatial correlations of density fluctuations are calculated as $g^{(2)}(y, y') = \langle \hat{\psi}^\dagger(y) \hat{\psi}^\dagger(y') \hat{\psi}(y') \hat{\psi}(y) \rangle / \langle \hat{n}(y) \rangle \langle \hat{n}(y') \rangle$, where $\langle \hat{n}(y) \rangle \equiv \langle \hat{\psi}^\dagger(y) \hat{\psi}(y) \rangle$, and the quantum expectation values can be calculated from Wigner averages $\langle \dots \rangle_W$ over a large number of independent stochastic

In the dilute limit of weak polariton-polariton interactions, the dynamics of the system can be accurately captured by a mean-field treatment where the quantum polariton field, $\hat{\psi}$, is approximated by a classical field equal to its expectation value, $\phi = \langle \hat{\psi} \rangle$. The evolution of such field is determined by a one-dimensional driven-dissipative nonlinear Schrödinger equation, or generalized Gross-Pitaevskii equation [1]:

evidencing the subsonic/supersonic transition of our analog black-hole event horizon.

VI. NUMERICAL SIMULATIONS II: SPATIAL CORRELATIONS

The horizon created at the engineered defect of our microwire is particularly promising for the experimental detection of spontaneous Hawking radiation by vacuum field fluctuations at the subsonic/supersonic boundary. An indirect experimental measure of such an emission can be performed by intensity correlation measurements at equal times. In order to estimate the feasibility of this experiment for the present horizon, we have calculated the density-density spatial correlations around the engineered defect, as shown in Fig. 4 of the main text.

To include the fluctuations of the polariton field around its mean value, we have employed a technique originally developed in a quantum optics context and then widely applied to dilute quantum fluids, the so-called *truncated Wigner approximation* [9, 10]. This technique was recently extended to treat out-of-equilibrium quantum fluids of polaritons in [5, 11]. In brief, the dynamics of the quantum field problem can be described by a stochastic partial differential equation of the form:

configurations [11], as obtained, e.g., by sampling the stochastic evolution at different times spaced by wide temporal intervals $T_s \gg 1/\gamma$. In particular, the average density is obtained as

$$\langle \hat{\psi}^\dagger(y) \hat{\psi}(y) \rangle = \langle |\phi(y)|^2 \rangle_W - \frac{1}{2\Delta y} \quad (\text{S9})$$

while the density correlation by:

$$\begin{aligned} \langle \hat{\psi}^\dagger(y) \hat{\psi}^\dagger(y') \hat{\psi}(y') \hat{\psi}(y) \rangle = \\ = \langle |\phi(y)|^2 |\phi(y')|^2 \rangle_W + \frac{1}{4\Delta y^2} (1 + \delta_{y,y'}) + \\ - \frac{1}{2\Delta y} (1 + \delta_{y,y'}) \langle |\phi(y)|^2 + |\phi_c(y')|^2 \rangle_W. \end{aligned} \quad (\text{S10})$$

The results shown in Fig. 4 have been obtained after averaging over 2×10^5 Montecarlo realizations.

VII. SPATIAL POSITION OF THE MAXIMUM CORRELATION SIGNAL

The first calculations of the density correlation signal in [12, 13] addressed the case of fluids whose density, flow velocity and interaction energy is spatially piecewise constant in both upstream and downstream regions. In such case, the intensity of the signal for the different processes was maximum on straight lines defined by same optical-path conditions. Locating the horizon at $y_{hor} = 0$, for standard Hawking processes ($u - d_2$ in the notation of [14]), this condition reads

$$\frac{y}{-c^d + v^d} = \frac{y'}{-c^u + v^u} \quad (y' < 0 < y) \quad (\text{S11})$$

while it reads

$$\frac{y}{-c^d + v^d} = \frac{y'}{c^d + v^d} \quad (0 < y, y') \quad (\text{S12})$$

$$\frac{y}{c^d + v^d} = \frac{y'}{-c^u + v^u} \quad (y' < 0 < y), \quad (\text{S13})$$

for other processes labelled as $d_1 - d_2$ and $u - d_1$ in [14], respectively.

When the flow velocity and/or the speed of sound are spatially varying, the above equations have to be modified into integrals. For instance, the standard Hawking processes are expected to give a maximum signal on the curve defined by the implicit integral equation

$$\int_{\approx 0}^y \frac{dY}{-c^d(Y) + v^d(Y)} = \int_{\approx 0}^{y'} \frac{dY}{-c^u(Y) + v^u(Y)} \quad (\text{S14})$$

Of course, this equation is valid only within a geometrical optics approximation where the spatial variations are assumed to be slow as compared to the wavelength of the Hawking phonons. While this condition can be reasonably valid away from the horizon, exact determination of the lower integration limit in the vicinity of the horizon point at $y = 0$ goes beyond this approximation. In Fig. 4 of the main text, the integration limits have been determined by hand, so to optimize agreement with the numerical result. In spite of this arbitrariness, the green line is in good agreement with the main fringe of standard Hawking correlations, i.e. the $u - d_2$ feature of Ref. 14. A similar calculation has been performed with

comparable success to obtain the black line for the $d_1 - d_2$ feature of Ref 14. The appearance of additional fringes parallel to the main ones (barely visible in [14]) can be explained in terms of the strong curvature of the $k_y < 0$ part of the Bogoliubov dispersion in the downstream region, and from the complex density and velocity profiles in the horizon region [15].

VIII. ESTIMATION OF THE INTEGRATION TIME IN THE PROPOSED CORRELATION EXPERIMENTS

In order to experimentally access the intensity correlation map of the polariton fluid, a very convenient and recently developed experimental technique based on a streak camera allows measuring statistics by taking correlations of different photocounts instead of just averages [16]. In this technique, the arrival time of photons on the photocathode of the streak camera is registered with a time resolution as small as 1 ps. One of the advantages of this technique is the following: since detection is given by a linear photocathode and a CCD, the arrival time from different points of the sample (in our case, e.g., points upstream and downstream from the horizon, respectively) can be registered simultaneously. From these images, the space- and time-resolved intensity correlation function, $g^{(2)}(y, y', t, t')$, can be reconstructed by performing a statistical analysis.

Figure 4 of the main text shows the expected equal-time (i.e., $t = t'$) correlation signal for the sample used in our experiments, where nominal parameters have been used in the simulations, as explained above. In order to observe the Hawking signal, it is required a sensitivity in $g^{(2)}(y, y')$ of $\sim 5 \times 10^{-5}$. If we concentrate on the emission from two specific points of the sample, y and y' , a signal to noise ratio of ~ 1 requires a total number of coincidences $1/(5 \times 10^{-5})^2 \sim 10^9$. Given the time resolution of the streak camera and its repetition rate, we estimate a detection of about 3000 two-photon coincidences per second for the typical photon emission rates of our experiment. This estimate implies about 100 hours of continuous measurements to resolve the expected correlation signal of the spontaneous Hawking emission process. We notice that such an estimate assumes ideal stability conditions of the experimental set-up, but we trust that this is within reach with available technology.

Finally, we notice that an optimization of the structure can greatly reduce the integration time. Two possible strategies include (i) reducing the microwire width and (ii) working at an exciton-cavity detuning closer to zero. Both approaches would result in a larger effective value of the polariton-polariton interaction constant. We estimate that by reducing the wire width by a factor of two and by working at zero detuning, the polariton interaction constant can be increased by an order of magnitude. Monte-Carlo simulations under such conditions (not shown) predict a Hawking signal as strong as

$g^{(2)}(y, y') - 1 \approx 5 \times 10^{-4}$, i.e. an order of magnitude larger than the one predicted for the current sample in Figure 4 of the main text. The above estimate adapted to this

situation predicts an integration time as low as ~ 22 minutes, with strongly reduced stability requirements for the realization of the proposed experiment.

-
- [1] I. Carusotto and C. Ciuti, *Rev. Mod. Phys.* **85**, 299 (2013).
- [2] M. Wouters and I. Carusotto, *Phys. Rev. B* **79**, 125311 (2009).
- [3] D. D. Solnyshkov, H. Flayac, and G. Malpuech, *Phys. Rev. B* **84**, 233405 (2011).
- [4] I. Carusotto and C. Ciuti, *Phys. Rev. Lett.* **93**, 166401 (2004).
- [5] D. Gerace and I. Carusotto, *Phys. Rev. B* **86**, 144505 (2012).
- [6] S. Finazzi and R. Parentani, *Phys. Rev. D* **83**, 084010 (2011).
- [7] E. Wertz, L. Ferrier, D. D. Solnyshkov, R. Johne, D. Sanvitto, A. Lemaitre, I. Sagnes, R. Grousseau, A. V. Kavokin, P. Senellart, G. Malpuech, and J. Bloch, *Nat. Physics* **6**, 860 (2010).
- [8] L. P. Pitaevskii and S. Stringari, *Bose Einstein Condensation* (Cambridge University Press, Cambridge, 2003).
- [9] M. J. Steel, M. K. Olsen, L. I. Plimak, P. D. Drummond, S. M. Tan, M. J. Collet, D. F. Walls, and R. Graham, *Phys. Rev. A* **58**, 4824 (1998).
- [10] A. Sinatra, C. Lobo, and Y. Castin, *J. Phys. B* **35**, 3599 (2002).
- [11] I. Carusotto and C. Ciuti, *Phys. Rev. B* **72**, 125335 (2005).
- [12] R. Balbinot, A. Fabbri, S. Fagnocchi, A. Recati, and I. Carusotto, *Phys. Rev. A* **78**, 021603(R) (2008).
- [13] I. Carusotto, S. Fagnocchi, A. Recati, R. Balbinot, and A. Fabbri, *New J. Phys.* **10**, 103001 (2008).
- [14] A. Recati, N. Pavloff, and I. Carusotto, *Phys. Rev. A* **80**, 043603 (2009).
- [15] I. Zapata, M. Albert, R. Parentani, and F. Sols, *New J. Phys.* **13**, 063048 (2011).
- [16] J. Wiersig, C. Gies, F. Jahnke, M. Aßmann, T. Berstermann, M. Bayer, C. Kistner, S. Reitzenstein, C. Schneider, S. Hofling *et al*, *Nature* **460**, 245 (2009).